Electrical-Transport Properties of Iodine-Doped Conducting Polyaniline

A. Sarkar,[1] P. Ghosh,[1] A. K. Meikap,[1] S. K. Chattopadhyay,[1] S. K. Chatterjee,[1] P. Chowdhury,[2] K. Roy,[2] B. Saha[2]

[1]*Department of Physics, National Institute of Technology, Durgapur, Deemed University, Mahatma Gandhi Avenue, Pin 713 209, West Bengal, India*
[2]*Department of Chemistry, Visva-Bharati, Santiniketan 731 235, West Bengal, India*

Received 13 February 2007; accepted 17 September 2007
DOI 10.1002/app.27615
Published online 12 February 2008 in Wiley InterScience (www.interscience.wiley.com).

ABSTRACT: We investigated the electrical-transport properties of hydroiodic acid doped polyaniline in the temperature range 77–300 K, applying magnetic field strength to a maximum of 1 T in the frequency range 20 Hz–1 MHz. The direct-current conductivity was explained by variable range hopping theory, and the direct-current magnetoconductivity, which was positive, was interpreted by orbital magnetoconductivity theory. The alternating-current (ac) conductivity was found to follow the universal dielectric response $\sigma'(f) \propto f^s$, where $\sigma'(f)$ is the frequency-dependent real part of the complex ac conductivity, f is the frequency, and s is the frequency exponent. The trend in the variation of s, the temperature dependence of the frequency exponent, corroborated the fact that the correlated barrier hopping was the dominating charge-transport mechanism. The ac conductivity also showed a positive variation with magnetic field, which could be interpreted by this theory. © 2008 Wiley Periodicals, Inc. J Appl Polym Sci 108: 2312–2320, 2008

Key words: charge transport; conducting polymers; dielectric properties

INTRODUCTION

The growing applications for conducting polymers in the form of batteries, electromagnetic interference shielding, molecular sensors, nonlinear optical devices, and microelectronic devices[1–8] are the compelling factors that have generated universal interest among researchers for the in-depth study of conducting polymers. Among the conducting polymers that have been investigated, polyaniline (PANI) is regarded as a material having high potential commercial applications because of its low production cost, high environmental stability, and excellent electrical, magnetic, and optical properties.[9–14] Pure polymers can be classified as insulating or noncrystalline semiconducting materials with very low charge carrier mobilities. Doping renders it a good conductor due to the delocalization of charge and spin along the backbone of the polymer.[15–25] The electrical conductivity of PANI is affected most by doping and medium, and many investigations have been carried out on doped PANI during the last few decades. Kahol and coworkers[26,27] argued that quasi one-dimensional (1D) variable range hopping (VRH) was responsible for conduction in doped PANI, whereas Sanjai et al.[28] observed three-dimensional (3D) VRH conduction in unblended PANI but 1D VRH for blended PANI. Ghosh et al.[23] claimed a transition from 3D VRH Mott to Efros-Shoklovskii at low temperatures. Wang and coworkers[29,30] were of the opinion that 1D conduction is important for the system with conducting chains totally isolated, but if the bundles are coupled, the 1D VRH conduction is not valid. They further established that for such a system, the carriers undergo 3D delocalization. This has given rise to a considerable controversy over the applications of quasi 1D and 3D VRH models for PANI samples. Only a more rigorous transport property study on PANI with different dopants can do away with such controversies over the electron-transport mechanism in PANI. Although many investigations on the structures and conduction mechanisms have been done on HCl-, H_2SO_4-, and HBF_4-doped PANI,[31–34] very few works have been done on hydroiodic acid (HI) doped PANI. Spectroscopic and electrical characterization on iodine-doped PANI was investigated by Ção et al.[35] They studied the variation of direct-current (dc) conductivity with the amount of dopant. Park et al.[36] also reported the variation of room-temperature conductivity and thermoelectric power with iodine concentration in PANI. Cruz et al.[37] synthesized iodine-doped PANI by a plasma polymerization process and studied the effect of relative humidity on the

Correspondence to: A. K. Meikap (ak_meikap@yahoo.com).
Contract grant sponsor: Ministry of Human Resource Development, Government of India; contract grant numbers: F.27-1/2002.TS.V (03/19/2002) and F.28-1/2003.TS.V (03/31/2003).

Journal of Applied Polymer Science, Vol. 108, 2312–2320 (2008)

electrical conductivity. Zeng and Ko[38,39] established the relationship between the structure and conductivity. They also reported that iodine-doped PANI did not absorb moisture readily in comparison with protonic acid doped PANI. This property is favorable for applications in microelectronic and nonlinear optical devices. Therefore, a detailed electrical-transport property study is essential on this system before we can be sure about its applications. However, there has been no such systematic study on the electrical transport of iodine-doped PANI in the literature.

In this article, we present the detailed electrical-transport properties, such as dc and alternating-current (ac) conductivity, magnetoconductivity, and dielectric response, of HI-doped PANI in the temperature range 77–300 K.

EXPERIMENTAL

Sample preparation

The middle fraction of the pure distillate of aniline (Merck, Mumbai/Kolkata, India) obtained by distillation over zinc dust for the preparation of PANI and distillate was collected and stored in a refrigerator, whereas potassium iodate (Lab Chemicals Industry, India), HI (55% Guaranteed Reagent; Merck, Mumbai, India), and sodium thiosulfate (Qualigens, India) were used as received.

The synthesis of the polymer was carried out in a three-necked, round-bottom flask that was kept at a constant temperature (0–30°C). Distilled water (22.5 mL), concentrated HCl (20 mL), and aniline (2.5 mL, 0.0275 mol) were put in the flask and stirred well; purified N_2 gas was passed through the flask for 0.5 h. Potassium iodate solution (25 mL; 0.0055 mol of KIO_3) was added slowly with vigorous stirring by a magnetic stirrer. The total volume of the reaction mixtures was brought to 100 mL with distilled water. Sodium thiosulfate (1 g) was added 0.5 h later after volume make up. The precipitated PANI salt was filtered after a specified time and then washed with distilled water until a constant mass was reached.

The pristine PANI salt was converted into the emeraldine base by treatment with 3% ammonium hydroxide for 4 h. The base was then washed with distilled water and dried at room temperature for 48 h under dynamic vacuum; it was then subjected to doping with various concentrations of HI.

Techniques

Fourier transform infrared (FTIR) spectra were recorded on a Shimadzu (model 8400S) (Kyoto, Japan) FTIR spectrometer in the range 450–4000 cm^{-1} with KBr pellets. Thermal degradation studies were performed under N_2 gas with a Shimadzu DT-30 instrument at heating rate of 10°C/min from room temperature to 500°C. The electrical conductivity of the samples was measured by a standard four-probe method after good electrical contact was ensured with a highly conducting graphite adhesive (Electrodag 5513, Acheson, Williston, VT) and fine copper wires as the connecting wires. The dc conductivity was measured with an $8\frac{1}{2}$-digit Agilent 3458A multimeter. The temperature dependence of the conductivity was studied with a liquid nitrogen cryostat. For the control and measurement of the temperature, we used a ITC 502S Oxford temperature controller. The temperature-dependent ac measurement was carried out with a 4284A Agilent impedance analyzer with variation in frequency to a maximum of 1 MHz. To measure the dc and ac response, we prepared the samples as pellets 1 cm in diameter by pressing the powder under a hydraulic pressure of 500 MPa. The capacitance [C_p (F)] and the dissipation factor (D) were measured at various frequencies and temperatures. The frequency-dependent real parts of the ac conductivity [$\sigma'(f)$] and dielectric constant [$\varepsilon'(f)$] were calculated with the following relations: $\sigma'(f) = 2\pi f C_p D d/A$ and $\varepsilon'(f) = C_p d/\varepsilon_o A$, respectively, where ε_o (dielectric permittvity in vacuum) is equal to 8.854 $\times 10^{-12}$ F/m; A and d are the area and thickness of the sample, respectively; and f is the frequency (Hz). The magnetoconductivity was measured in the same manner by the variation of the transverse magnetic field (magnetic field (B) < 1 T) with an electromagnet.

RESULTS AND DISCUSSION

Thermal properties

Thermogravimetric analyses (TGAs) of two representative samples, PANI and PANI–HI4, are given in Figure 1. The mass loss of the PANI samples began around 50°C and continued until around 175°C; this

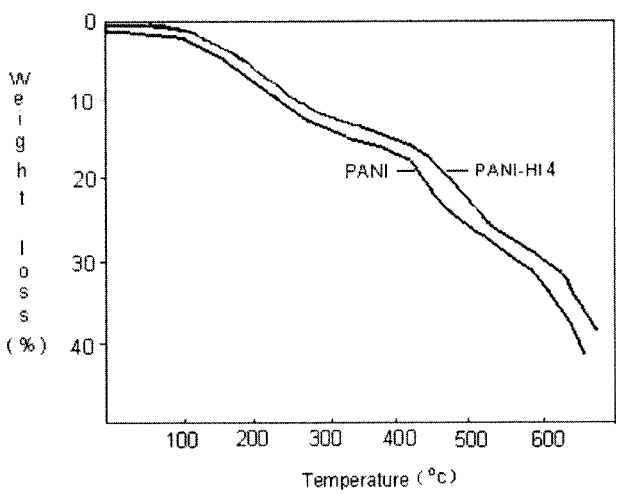

Figure 1 TGA curves of PANI and PANI–HI4.

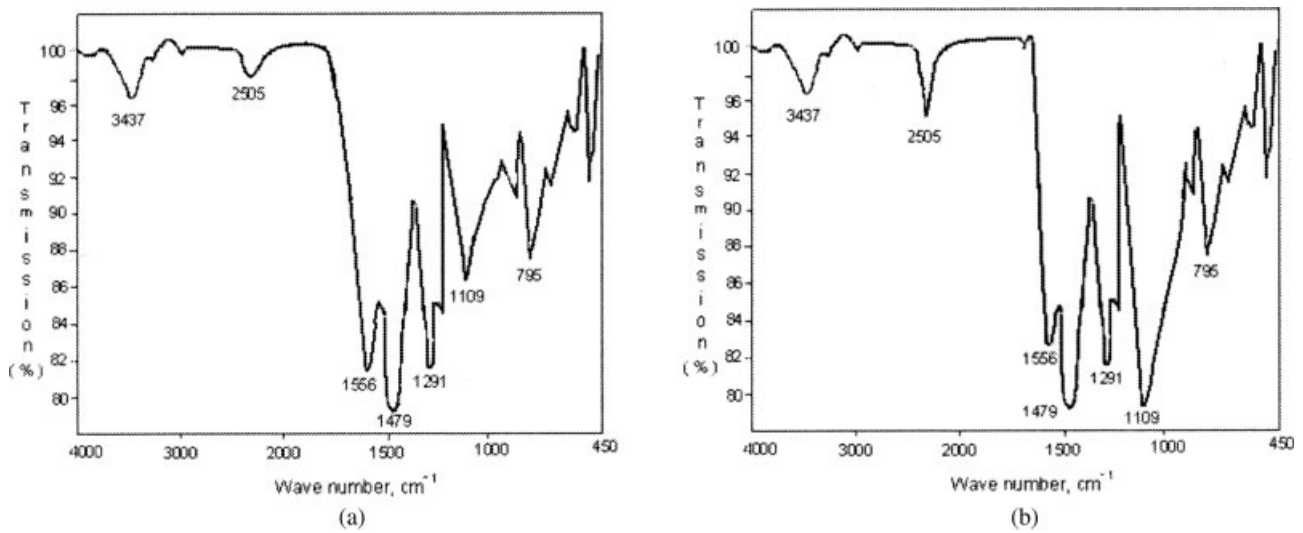

Figure 2 FTIR spectra of (a) PANI and (b) PANI–HI4.

was followed by a process of rapid mass loss up to a temperature of 500°C. The initial mass loss was due to the loss of water molecules, and the next stage was due to the oxidative degradation of the polymer in air. The sample PANI–HI4 showed a similar type of thermal degradation. However, the mass loss up to 205°C in this case was less than that of PANI, which indicated a better stability for PANI–HI4. The better thermal stability of PANI–HI4 could be explained by the dominancy of the benzinoid structure. Alternatively, the inferior thermal stability of PANI was due to the presence of a quinoid ring in its structure.

FTIR spectral analysis

The FTIR spectrum of PANI (Emeraldine base) is shown in Figure 2(a). The spectrum exhibited several characteristics peaks at 3437, 2505, 1556, 1479, 1291, 1109, and 795 cm^{-1}. These peaks were attributed to the NH stretching of secondary amine,[40] NH^+ stretching of amine,[41] quinoid ring stretching,[42–44] benzenoid ring stretching,[43–45] C—N stretching band,[46] vibrations of the dopant anion,[41,42] and para-disubstituted benzene,[47,48] respectively. The peak assignment revealed that the produced product was PANI, and it had the following structure (B represents the benzinoid ring, and Q represents the quinoid ring):

$$—B—N^{\bullet\bullet}\,H—B—N^{\bullet\bullet}H—B—N{=}Q{=}N—$$

The FTIR spectrum of PANI–HI4 is shown in Figure 2(b). The increase in area under the peaks at 2505 and 1109 cm^{-1} and the decrease in peak area at 1556 cm^{-1} with respect to the spectrum of PANI indicated the structural change in the polymer due to doping. The structure of HI-doped PANI may be represented as follows:

$$—B—N^{\bullet+}\,H—B—N^{\bullet\bullet}H—B—N^{\bullet+}H—B—N^{\bullet\bullet}H—$$

The TGA data (Fig. 1) showed a 2.5% weight loss due to the removal of water from 50 to 175°C. Thus, the water content of the sample PANI–HI4 was 2.5%. The FTIR spectra of the sample was taken with KBr pellets. The KBr pellets were prepared by the mixture of the sample with KBr (spectroscopic grade) in a 1 : 100 weight ratio to get a clear spectrum. Thus, the water content in the KBr pellets was less than 0.025%. The presence of a very small amount of water in the KBr pellets was evident from the small humps (weak peak) in the region 3650–3750 and 1596 cm^{-1} in Figure 2. Because the water content was very small, the area under the peaks and the intensity of the peaks were low.

dc conductivity

The electrical dc conductivity [$\sigma(T)$] for the different HI-doped PANI samples was measured in the temperature range 77–300 K. The room-temperature conductivity σ(300 K) is listed in Table I; it varied between 1.87×10^{-5} and 1.08×10^{-3} Ω^{-1} cm^{-1}. Similar variations in conductivity with iodine content were observed by Zeng and Ko.[38] They showed that conductivity increased rapidly with iodine content and reached a maximum value of 1.83×10^{-3} Ω^{-1} cm^{-1}. In our investigation, the rapid increase in the conductivity of PANI–HI4 was due to the presence of more iodine in PANI when it was doped with HI of higher concentration. Figure 3 shows the temperature dependence of $\sigma(T)$ of different samples. The samples exhibited nonmetallic (semicon-

TABLE I
Different Physical Parameters of the PANI Samples

Parameter	PANI–HI1	PANI–HI2	PANI–HI3	PANI–HI4
x (N)[a]	0.5	1.0	2.0	2.5
σ(300 K) (Ω^{-1} cm^{-1})	1.87×10^{-5}	2.45×10^{-5}	2.87×10^{-5}	1.08×10^{-3}
ρ_r	1.38	1.79	3.17	58.45
γ	1/4	1/4	1/4	1/4
T_o (K)	4.135×10^{3}	2.997×10^{4}	1.259×10^{5}	3.479×10^{6}
L_{loc} (Å)	452.60	365.60	205.28	72.57
C_{sat}	2.49×10^{-3}	9.41×10^{-2}	2.14×10^{-1}	7.43×10^{-1}
$N(E_F)$ (states/eV^{-1} cm^{-3})	4.839×10^{17}	1.267×10^{17}	1.703×10^{17}	1.395×10^{17}
τ_o (s)	7.01×10^{-8}	8.04×10^{-8}	9.42×10^{-8}	2.28×10^{-7}
W_m (eV)	0.471	0.456	0.438	0.419
ε_∞	124.69	95.86	48.42	35.10
ε_s	5071.65	1087.92	253.24	200.93
τ (s)	2.61×10^{-3}	2.52×10^{-3}	1.46×10^{-3}	1.05×10^{-3}

[a] Concentration of HI.

ducting) temperature dependence; that is, the conductivity increased with increasing temperature. A hopping-type temperature dependence for the conductivity can be attributed to such a system. According to this model,[49,50] the conductivity is given by

$$\sigma(T) = \sigma_o(T_o/T)^{1/2} \exp[-(T_o/T)^{\gamma}] \quad (1)$$

$$T_o = 16/[k_B N(E_F) L_{loc}{}^3] \quad (2)$$

where γ is the VRH exponent, which indicates the dimensionality of the conducting medium; T_o is the Mott characteristic temperature; T is the temperature; σ_o is the conductivity at an infinite temperature; k_B is the Boltzmann constant; $N(E_F)$ is the density of states at the Fermi level; and L_{loc} is the localization length. The possible values of γ were 1/4, 1/3, and 1/2 for the 3D, 2D, and 1D systems, respectively. We plotted $\ln[T^{1/2}\sigma(T)]$ as a function of $T^{-1/4}$. This plot exhibited a straight-line behavior for all of the samples, as shown in Figure 3. From the slope of the straight lines, the values of the parameter T_o were evaluated and are listed in Table I. The values of T_o strongly depended on the resistivity ratio [ρ_r = σ(300 K)/σ(77 K), where σ(77 K) is the conductivity at 77 K], and its value varied from 4.135×10^3 to 3.479×10^6 K with the variation of ρ_r from 1.38 to 58.45. Therefore, it was concluded from the value of γ, which turned out to be 1/4 for all of the samples, that 3D conduction hopping may have dominated for these investigated samples in the temperature range 77–300 K.

Figure 4 shows the variation of magnetoconductivity with magnetic field of different samples at 200 K. All of the samples showed positive magnetoconductivity, whereas the HCl- and H_2SO_4-doped PANI showed negative magnetoconductivity.[23] According to VRH theory, conductivity in the presence of a

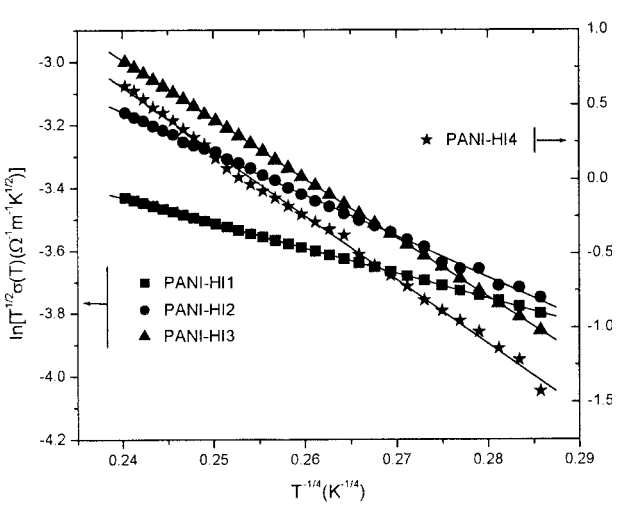

Figure 3 Temperature dependence of the dc conductivity of HI-doped PANI samples. The solid lines are fitted to eq. (1).

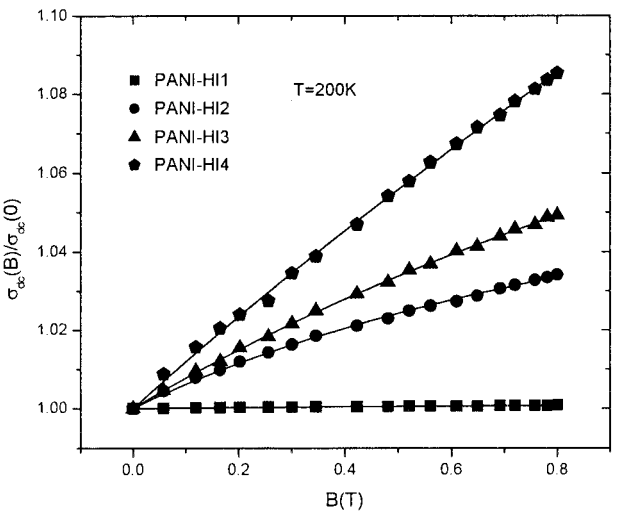

Figure 4 Variation of the dc magnetoconductivity with the magnetic field of HI-doped PANI samples at 200 K. The solid lines are fitted to eq. (3).

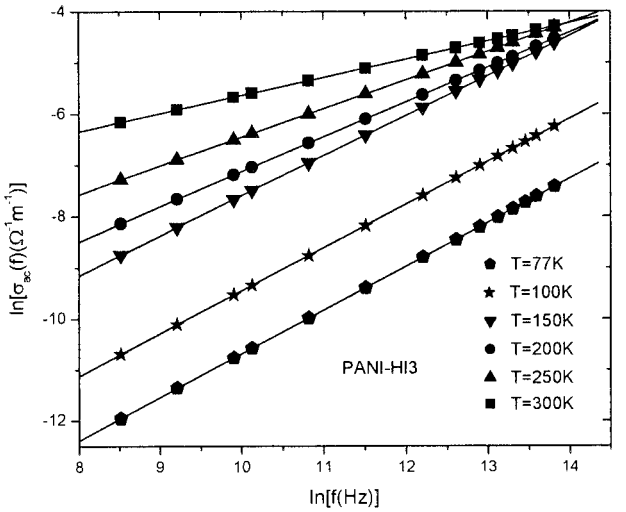

Figure 5 Frequency dependence of the ac conductivity of PANI–HI3 at different temperatures.

magnetic field can be explained by two mechanisms, such as the wave function shrinkage model[51–55] and orbital magnetoconductivity theory.[56–58] As per the wave function shrinkage model, the application of the magnetic field reduces the overlapping probability between two sites, which results in negative magnetoconductivity. However, orbital magnetoconductivity theory takes into account the forward interference among the random paths in the hopping process between two sites spaced at a distance equal to the optimum hopping distance, and the theory predicts positive magnetoconductivity, which is expressed as[56–58]

$$\sigma(B,T)/\sigma(0,T) = 1 + (C_{\text{sat}}B/B_{\text{sat}})/(1 + B/B_{\text{sat}}) \quad (3)$$

where $\sigma(B,T)$ is conductivity at magnetic field B, $\sigma(0,T)$ is conductivity at zero magnetic field, B_{sat} (magnetic field at which the magnetoconductivity is saturated) is equal to $0.7(h/e)(8/3)^{3/2}(1/L_{\text{loc}}{}^2)(T/T_o)^{3/8}$ and C_{sat} is a temperature-independent parameter. Because the observed magnetoconductivities of the investigated samples were positive, we analyzed the measured data with the help of orbital magnetoconductivity theory. The different points in Figure 4 are the experimental data for different samples, whereas the solid lines represent the best fits obtained from eq. (3), with C_{sat} and L_{loc} taken as the fitting parameters and with the value of T_o, obtained from dc conductivity data. As shown in Figure 4, it was evident that the experimental data could well describe the theory, as indicated in eq. (3). The best fitted values of L_{loc} and C_{sat} are listed in Table I. L_{loc} gradually decreased with increasing ρ_r. As the extent of disorder is generally characterized in terms of ρ_r, the higher value of ρ_r implied the presence of more disorder in the samples, due to which the electronic wave functions was localized within a small region, which led to the shortening of L_{loc} with increasing ρ_r. With the values of T_o and L_{loc} for different samples in eq. (2), the values of $N(E_F)$ were calculated and are listed in Table I.

ac conductivity

The frequency-dependent conductivity of the investigated samples were investigated in the frequency 20 Hz–1 MHz and in the temperature range 77–300 K. It has been shown for many amorphous semiconductors or disordered systems that in addition to the dc conductivity contribution (σ_{dc}), $\sigma'(f)$ follows so-called universal dielectric response behavior, which can be expressed as[49,59,60]

$$\sigma'(f) = \sigma_{dc} + \sigma_{ac}(f) = \sigma_{dc} + \alpha f^s \quad (4)$$

where $\sigma_{ac}(f)$ is ac conductivity, α is the temperature-dependent constant, f is the measuring frequency, and the frequency exponent s is less than or equal to 1. The measured data showed that at higher frequencies, the conductivity followed the power law, whereas at lower frequencies, the data bent away from this dependence; this could be attributed to the dc contribution. We calculated the frequency-dependent part [$\sigma_{ac}(f)$] by subtracting σ_{dc} from $\sigma'(f)$. Figure 5 shows the variation of ln[$\sigma_{ac}(f)$] with ln(f) at different temperatures for the sample PANI–HI3. Similar behavior was observed for all other samples. The value of s was calculated from the slope of ln[$\sigma_{ac}(f)$] versus ln(f) plot for different samples at each temper-

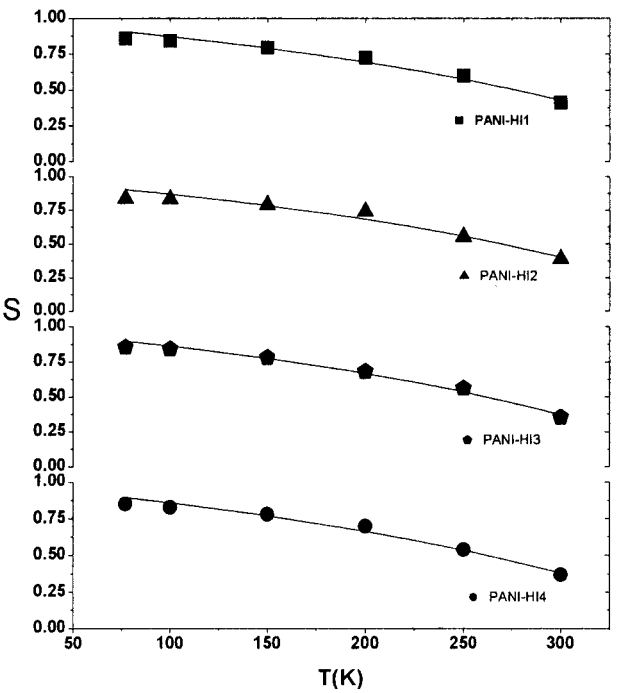

Figure 6 Variation of frequency exponent s with temperature T of different HI-doped PANI samples.

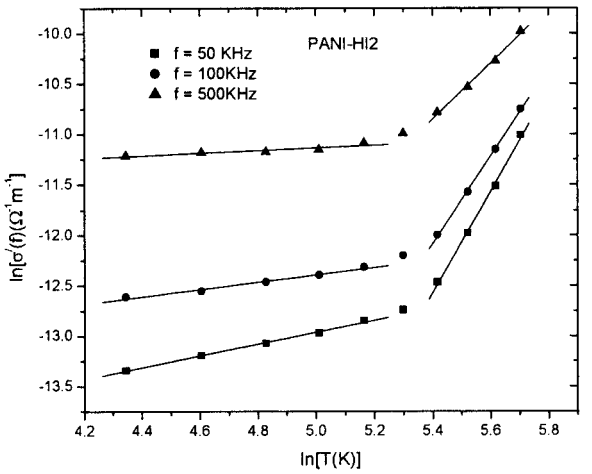

Figure 7 Variation of $\sigma'(f)$ as a function of temperature T at different frequencies for sample PANI–HI2.

ature. The temperature dependences of s are shown in Figure 6. As shown in Figure 6, it became evident that the estimated values of s gradually decreased with increasing temperature. Although the charge transport of disordered systems is governed by two physical processes, such as correlated barrier hopping (CBH)[60] and quantum mechanical tunnelling,[59–61] this type of temperature dependency of the frequency exponent s is only observed in the CBH model.[60] According to this model, s can be expressed as

$$s = 1 - 6k_bT/[W_m - k_bT\,\mathrm{in}(1/\omega\tau_o)] \quad (5)$$

where W_m is the effective barrier height at infinite intersite separation, ω is the ac frequency, and τ_o is the characteristic relaxation time. We are aware that the model predicts both the temperature and frequency dependence of s. For small values of W_m/k_BT, s increases with increasing frequency, but for large values of W_m/k_BT, the variation of s is so small that it is in effect independent of frequency.[31] On the other hand, we observed in our study that s was independent of frequency (Fig. 5). Therefore, the values of W_m and τ_o were obtained by the best fitted parameters to eq. (5) at a frequency of 1 kHz and are given in Table I. Figure 6 shows that the experimental values of s were in good agreement with the theoretical model. Therefore, from the trend of variation of s with temperature as presented in Figure 6, we concluded that the ac conductivity in the investigated samples was described by the CBH model.

Figure 7 shows the variation of ac conductivity with temperature for the sample PANI–HI2 for different yet constant frequencies. The ac conductivity increased monotonically with temperature and also with increased frequency for all the investigated samples. According to the CBH model,[49,60,61] the temperature dependence of $\sigma'(f)$ is expressed as $\sigma'(f) \propto T^n$ where $n = (1 - s)\ \ln(1/\omega\tau_o)$ for the narrow band limit and $n = 2 + (1 - s)\ \ln(1/\omega\tau_o)$ for the broad band limit. Figure 7 shows two types of slopes throughout the investigated temperature range for each frequency. We calculated the values of n from the slope of the $\ln[\sigma'(f)]$ versus $\ln T$ plot for each frequency in the two temperature ranges. With increasing frequency from 50 to 500 kHz, the values of n varied from 0.56 to 0.1 in the temperature range 77–150 K and from 5.03 to 2.78 in the temperature range 225–300 K. This indicated that n depended on frequency as well as range of temperature. According to the theory, the value of n also increases with temperature (as s decreases with temperature) and decreases with increasing frequency. We calculated the values of n theoretically by taking $\tau_o = 8.04 \times 10^{-8}$ s and the value of s of 0.39 for 300 K and 0.84 for 77 K for different frequencies. According to the narrow band limit, the values of n varied from 2.25 to 0.84 for 300 K and 0.61 to 0.23 for 77 K with increasing frequency from 50 to 500 kHz; on the other hand, the values of n varied from 4.25 to 2.84 for 300 K and from 2.605 to 2.226 for 77 K with increasing frequency from 50 to 500 kHz for the broad band limit. We observed that the experimental values were close to the values obtained from the broad band limit in the temperature range 225–300 K, but at low temperatures (77–150 K), the values of n were close to the values obtained from the narrow band limit. Generally, the narrow band limit is applicable above room temperature; however, the broad band limit was applicable below room temperature. Hence below room temperature, the applicability of narrow band limit led to the anomalous behavior of n. Therefore, a more explicit study is necessary to understand such anomalous behaviors of n below room temperature for this system.

Figure 8 shows the variation in $\sigma'(f)$ with the transverse magnetic field of the different HI-doped

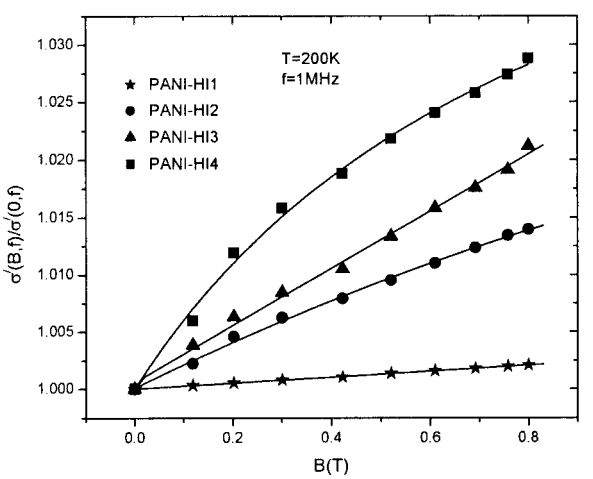

Figure 8 Magnetic field dependence of the ac conductivity of different samples at 200 K.

PANI samples at 200 K. All of the investigated samples showed positive ac magnetoconductivity. There is no theoretical model in the literature to explain directly the behavior of ac conductivity in the presence of a magnetic field. Catalan[62] pointed out that magnetic field dependence dielectric response occurs in materials in which a region exists with different dc magnetoconductance responses. He explained the magnetodielectric effects by using the Maxwell–Wagner effect in combination with the dc magnetoconductance for samples having a heterogeneous nature, that is, a mixture of insulating and metallic regions. The model consists of two leaky capacitors in series with one of the leakage components being magnetically tunable. If the conductance of any of the layers is changed by a magnetic field, that will affect the measured dielectric response. He also pointed out that the sign of the magnetocapacitance depends on the sign of the dc magnetoconductance occurring at the interface or at the core. As $\sigma'(f)$ is related to the dielectric response [$\sigma'(f) = 2\pi f C_p D d / A$], the application of a magnetic field also affects the ac conductivity. As shown in Figure 4, the measured dc magnetoconductivity was positive, that is, of same sign as that of the ac magnetoconductivity. On the other hand, the 3D hopping of dc conductivity suggested the presence of conducting islands between the insulating matrix; that is, samples contained regions of different magnetoconductance responses, and the dielectric permittivity of the samples were also well explained by the Maxwell–Wagner capacitor model (details later). Therefore, we concluded that the observed influence of magnetic field on the ac conductivity may have been due to the combined effects of the dc magnetoconductance and the Maxwell–Wagner effect.

Dielectric permittivity

The variation of $\varepsilon'(f)$ as a function of frequency is given in Figure 9 for different samples at 200 K and in the inset of Figure 9 for PANI–HI1 at different constant temperatures. $\varepsilon'(f)$ approached a limiting constant value at high frequencies; this arose from rapid polarization processes occurring in the material. The sudden increase in the value of $\varepsilon'(f)$ at low frequency indicated the presence of a large degree of dispersion due to charge transfer within the interfacial diffusion layer present between the electrodes.[63,64] As shown in the inset of Figure 9, the rapid increase in $\varepsilon'(f)$ occurred at high frequency with increasing temperature. This was because the magnitude of the dielectric dispersion was temperature-dependent. At lower temperatures, the freezing of the electric dipoles through the relaxation process was easier. So when dispersion was observed at lower frequency but high temperature, the rate of polarization was rapid, and this caused the relaxation at high frequency. The effective dielectric permittivity of inhomogeneous systems consisting of different permittivities and conductivities is given by the Maxwell–Wagner capacitors model:[65–67]

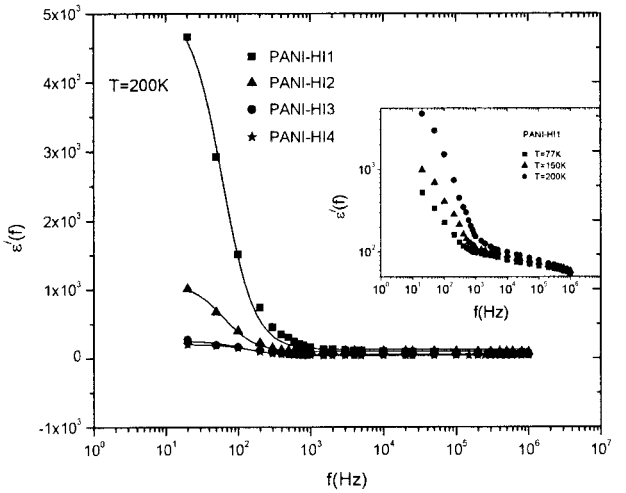

Figure 9 $\varepsilon'(f)$ as a function of f at 200 K of different samples. The inset shows the variation of $\varepsilon'(f)$ as a function of f at different temperatures of PANI–HI1.

$$\varepsilon(\omega) = \varepsilon'(\omega) - i\varepsilon''(\omega) = \varepsilon_\infty + (\varepsilon_s - \varepsilon_\infty)/(1 + i\omega\tau) - i\sigma/\omega \quad (6)$$

where $\varepsilon''(\omega)$ is the imaginary part of dielectric permittivity, ε_∞ and ε_s are the dielectric permittivities at infinite frequency and low frequency, respectively; θ is the average relaxation time; and σ is the dc conductivity. In Figure 9, the points are the experimental data for the different samples, and the solid lines are the theoretical values obtained from the real part of eq. (6). As shown in Figure 9, the experimental data were reasonably well fitted with the theory. The best fitted parameters are shown in Table I. Generally, the resistance and capacitance of the interfacial grain boundary (R_{gb} and C_{gb}, respectively) are larger than those of the grain (R_g and C_g, respectively), that is, $R_{gb} \gg R_g$ and $C_{gb} \gg C_g$. Under these conditions, the expressions for ε_∞ and ε_s are reduced to C_g/C_0 and C_{gb}/C_0. Where C_0 is the capacity in free space. Therefore, we concluded that the permittivity was dominated by grain boundary behavior at low frequency and by the grain phase at high frequency.

CONCLUSIONS

The dc conductivity and ac conductivity of HI-doped PANI samples were examined at temperatures between 77 and 300 K and in the presence of a magnetic field of a maximum of 1 T. The dc conductivity of all of the samples increased with increasing tem-

perature; that is, the temperature coefficient of resistivity was negative. In this temperature range, the dc conductivity followed the 3D Mott VRH conduction. The dc magnetoconductivity of the samples was positive, which was explained by orbital magnetoconductivity theory. $\sigma'(f)$ was found to follow the universal dielectric response $\sigma'(f) \propto f^s$. A detailed analysis of the temperature dependence of the universal dielectric response parameter s revealed that the correlated barrier hopping was the dominating charge-transport mechanism. The temperature dependence of the ac conductivity obeyed the power law $\sigma'(f) \propto T^n$; the magnitude of the temperature exponent n strongly depended on the frequency and range of temperature. The ac conductivity showed positive variation in the presence of a magnetic field. This behavior could be explained by the Maxwell–Wagner effect combined with dc magnetoconductivity. $\varepsilon'(f)$ showed a large degree of dispersion at low frequency but rapid polarization at high frequencies, which was described by the Maxwell–Wagner capacitor model. Different physical parameters, such as $N(E_F)$, L_{loc}, W_m, and τ_o were determined from the experimental data with VRH theory.

The authors gratefully acknowledge the principal assistance received from Ministry of Human Resource Development, Government of India, during this work.

References

1. Naarman, H. Science and Application of Conducting Polymers; Adam Hilger: Bristol, 1991.
2. Genies, E. M.; Hany, P.; Santier, C. J Appl Electrochem 1988, 18, 751.
3. Joo, J.; Epstein, A. J. Appl Phys Lett 1994, 65, 2278.
4. Bartlett, P. N.; Birkin, P. R. Synth Met 1993, 61, 15.
5. Osaheni, J. Á.; Jenekhe, A. S.; Vanherzeele, H.; Meth, J. S.; Sun, Y.; MacDiarmid, A. G. J Phys Chem 1992, 96, 2830.
6. Kobayashi, T.; Yoneyama, H.; Tamura, H. J Electroanal Chem 1984, 161, 419.
7. Hau, Z.; Shi, J.; Zhang, L.; Ruan, M.; Yan, J. Adv Mater 2002, 14, 830.
8. Levi, B. G. Phys Today 2000, 53, 19.
9. Genies, E. M.; Boyle, A.; Lapkowski, M.; Tsintavis, C. Synth Met 1990, 36, 139.
10. MacDiarmid, A. G.; Chiang, J. C.; Halpern, M.; Haung, W. S.; Um, S. L.; Somasiri, N. L. D.; Wu, W. Q.; Yaninger, S. Z. Mol Cryst Liq Cryst 1985, 121, 173.
11. Chiang, J. C.; MacDiarmid, A. G. Synth Met 1986, 13, 193.
12. Skothemin, T.; Elsenbaumer, R. Handbook of Conducting Polymers; Marcel Dekker: New York, 1998.
13. MacDiarmid, A. G. Conjugated Polymers and Related Materials; Oxford University Press: London, 1993.
14. Seanor, D. A. Electronic Properties of Polymers; Academic: New York, 1992.
15. Ghosh, M.; Barman, A.; Das, A.; Meikap, A. K.; De, S. K.; Chatterjee, S. J Appl Phys 1998, 83, 4230.
16. Burroughes, J. H.; Bradely, D. C.; Brown, A. R.; Marks, R. N.; Mackey, K.; Friend, R. H.; Bruns, P. L. Nature 1990, 347, 539.
17. Chien, W. C. Polyacetylene; Academic: New York, 1984.
18. Jin, Z.; Su, Y.; Duan, Y. Sensors Actuators B 2001, 72, 75.
19. Sotomayor, P. T.; Raimurdo, I. M., Jr.; Zarbin, A. J. G.; Rohwedder, J. J. R.; Netto, G. O.; Alves, O. L. Sensors Actuators B 2001, 74, 157.
20. Kane-Magurie, L. A. P.; Wallasce, G. G. Synth Met 2001, 119, 39.
21. Hamers, R. J. Nature (London) 2001, 412, 489.
22. Rosseinssky, D. R.; Mortimer, R. J. Adv Mater 2001, 13, 783.
23. Ghosh, M.; Barman, A.; Meikap, A. K.; De, S. K.; Chatterjee, S.; Chattopadhyay, S. K. J Appl Polym Sci 2000, 75, 1480.
24. Sarkar, A.; Ghosh, P.; Meikap, A. K.; Chattopadhyay, S. K.; Chatterjee, S. K.; Ghosh, M. J Appl Phys 2005, 97, 113713.
25. Ghosh, P.; Sarkar, A.; Meikap, A. K.; Chattopadhyay, S. K.; Chatterjee, S. K.; Ghosh, M. J Phys D: Appl Phys 2006, 39, 3047.
26. Kahol, P. K.; Pinto, N. J.; Berndtsson, E. J.; Mccormic, B. J. J Phys: Condens Matter 1994, 6, 5631.
27. Kahol, P. K.; Pendse, V.; Pinto, N. J.; Traore, M.; Stevenson, W. T. K.; Mccormick, B. J.; Gundersen, J. N. Phys Rev B 1994, 50, 2809.
28. Sanjai, B.; Roghunathan, A.; Natarajan, T. S.; Rangarajan, G. Phys Rev B 1997, 55, 10734.
29. Wang, Z. H.; Scherr, E. M.; MacDiarmid, A. G.; Epstein, A. J. Phys Rev B 1992, 45, 4190.
30. Wang, Z. H.; Li, C.; Scherr, E. M.; MacDiarmid, A. G.; Epstein, A. J. Phys Rev Lett 1991, 66, 1745.
31. Ghosh, M.; Barman, A.; De, S. K.; Chatterjee, S. J Appl Phys 1998, 84, 806.
32. Inoue, M.; Navarro, R. E.; Inoue, M. B. Synth Met 1989, 30, 199.
33. MacDiarmid, A. G.; Chiang, J. C.; Richter, A. F.; Epstein, A. J. Synth Met 1987, 18, 285.
34. Li, W.; Zhang, Q.; Chen, D.; Li, L. J Macromol Sci Pure Appl Chem 2006, 43, 1815.
35. Ção, Y.; Li, S.; Xue, Z.; Guo, D. Synth Met 1986, 16, 305.
36. Park, Y. W.; Moon, J. S.; Bak, M. K.; Jin, J. I. Synth Met 1989, 29, 389.
37. Cruz, C. J.; Morales, J.; Castillo-Ortega, M. M.; Olayo, R. Synth Met 1997, 88, 213.
38. Zeng, X. R.; Ko, T. M. J Polym Sci Part B: Polym Phys 1997, 35, 1993.
39. Zeng, X. R.; Ko, T. M. Polymer 1998, 39, 1187.
40. Kalsi, P. S. Spectroscopy of Organic Compounds, 6th ed.; New Age International: New Delhi, 2004; p 111.
41. Athawale, A. A.; Chabukswar, V. V. J Appl Polym Sci 2001, 79, 1994.
42. Palaniappan, S. Eur Polym J 2001, 37, 975.
43. Zhang, Z.; Wei, Z.; Wan, M. Macromolecules 2002, 35, 3967.
44. Marie, E.; Rothe, R.; Antonietti, M.; Landfester, K. Macromolecules 2003, 36, 3967.
45. Ruckenstein, E.; Yin, W. J Appl Polym Sci 2001, 79, 80.
46. Athawale, A. A.; Kulkarni, M. V.; Chabukswar, V. V. Mater Chem Phys 2002, 73, 106.
47. Dyer, J. R. Application of Absorption Spectroscopy of Organic Compounds; Prentice Hall of India: New Delhi, 1991; p 36.
48. Campos, T. L. A.; Kersting, D. F.; Ferreira, C. A. Surface Coat Technol 1997, 122, 3.
49. Mott, N. F.; Davis, E. Electronics Process in Nanocrystalline Materials, 2nd ed.; Clarendon: Oxford, 1979.
50. Friedman, L.; Pollak, M. Phil Mag B 1978, 38, 173.
51. Tokumoto, H.; Mansfield, R.; Lea, M. J. Phil Mag B 1982, 46, 93.
52. Shklovskii, B. I. Sov Phys JETP Lett 1982, 36, 51.
53. Shklovskii, B. I. Sov Phys Semicond 1983, 17, 1311.
54. Shklovskii, B. I.; Efroa, A. L. Electronic Properties of Doped Semiconductors; Springer: Berlin, 1984; p 202.

55. Schoepe, W. Z Phys B 1988, 71, 455.
56. Nguyen, V. L.; Spivak, B. Z.; Shklovskii, B. I. JETP Lett 1985, 41, 42.
57. Nguyen, V. L.; Spivak, B. Z.; Shklovskii, B. I. Sov Phys JETP 1985, 62, 1021.
58. Sivan, U.; Entin-Wohiman, O.; Imry, Y. Phys Rev Lett 1988, 60, 1566.
59. Long, A. R. Adv Phys 1982, 31, 553.
60. Elliott, S. R. Adv Phys 1987, 36, 135.
61. Efros, A. L. Phil Mag B 1981, 43, 829.
62. Catalan, G. Appl Phys Lett 2006, 88, 102902.
63. Cole, K. S.; Cole, R. H. J Chem Phys 1941, 9, 441.
64. Frohlieh, H. Theory of Dielectrics; Oxford University Press: London, 1958.
65. Maxwell, J. C. A Treatise on Electricity and Magnetism; Oxford University Press: Oxford, 1988; Vol. 1.
66. Wagner, K. W. Annu Phys (Lpz) 1913, 40, 53.
67. Hippel, V. Dielectrics and Waves; Wiley: New York, 1954.